



# EES Solar

# **Accepted Manuscript**

This article can be cited before page numbers have been issued, to do this please use: E. L. Quinn, H. Lohan, E. Tmava, S. Dong, A. Walsh and R. L. Z. Hoye, *EES Sol.*, 2025, DOI: 10.1039/D5EL00157A.



This is an Accepted Manuscript, which has been through the Royal Society of Chemistry peer review process and has been accepted for publication.

Accepted Manuscripts are published online shortly after acceptance, before technical editing, formatting and proof reading. Using this free service, authors can make their results available to the community, in citable form, before we publish the edited article. We will replace this Accepted Manuscript with the edited and formatted Advance Article as soon as it is available.

You can find more information about Accepted Manuscripts in the <u>Information for Authors</u>.

Please note that technical editing may introduce minor changes to the text and/or graphics, which may alter content. The journal's standard <u>Terms & Conditions</u> and the <u>Ethical guidelines</u> still apply. In no event shall the Royal Society of Chemistry be held responsible for any errors or omissions in this Accepted Manuscript or any consequences arising from the use of any information it contains.



View Article Online DOI: 10.1039/D5EL00157A

Solar absorbers that are simultaneously efficient and able to be manufactured cost-effectively have long been sought after. Lead-halide perovskites (LHPs) were a surprising discovery that fulfils these requirements, and are now entering into commercial production. However, the toxicity and limited ambient stability of LHPs have prompted a search for alternatives that could mimic their exceptional optoelectronic properties, whilst overcoming their limitations. Most 'perovskite-inspired' materials thus far have yielded power conversion efficiencies (PCEs) <10% in solar cells. It is therefore remarkable that CsBiSCl<sub>2</sub> was recently reported to achieve 10.38% PCE under 1-sun illumination, and maintain 97% of its original PCE after 150 days of storage in air without encapsulation. CsBiSCl<sub>2</sub> is also free from any toxic elements, and is reported to have a bandgap of 2.0 eV, which is ideal for applications as top-cell in tandem photovoltaics, for indoor photovoltaics, or for photoelectrochemical cells. However, the structure and synthesis of the material are poorly evidenced and understood. Herein, we use computational investigations to rigorously determine the lowest-energy structure for CsBiSCl<sub>2</sub>, and we show that the original synthesis method reported does not yield CsBiSCl<sub>2</sub> thin films. We find the claimed 10.38% PCE to be spurious and recommend that the field avoids investing research efforts towards this material. In particular, we find that the lowest-energy structure of CsBiSCl<sub>2</sub> is above the convex hull, making it challenging to avoid phase impurities from the Cs-Bi-S-Cl family of materials.

Solar Accepted Manusc

View Article Online DOI: 10.1039/D5EL00157A

# **ARTICLE**

# Evaluating the Potential of CsBiSCl<sub>2</sub> as a Solar Absorber

computational results together, it is unlikely that >10%-efficient CsBiSCl<sub>2</sub> solar cells have been achieved.

Eilidh L. Quinn, at Hugh Lohan, a,bt Elita Tmava, a Shiling Dong, Aron Walshb, and Robert L. Z. Hoye \*a

Efforts to develop lead-free and stable alternatives to halide perovskites have thus far mostly yielded materials with power conversion efficiencies (PCEs) well below 10% in solar cells. Recently, photovoltaics based on CsBiSCl<sub>2</sub> were reported to achieve 10.38% PCE. Still, the crystal structure is unknown, and it is unclear whether the reported thin film synthesis method could realize thin films with the desired phase and stoichiometry. Herein, we use *ab-initio* Random Structure Searching (AiRSS) with a bespoke machine learned interatomic potential to explore the potential energy surface of CsBiSCl<sub>2</sub>, finding the previously-proposed cubic perovskite structure to be implausible. The lowest-energy structure we find is a four formula unit orthorhombic structure (*Pnma* space group) that lies 2.4 meV/atom above the convex hull. There is strong competition in the Cs-Bi-S-Cl family, which can lead to phase impurities. By examining the reported solution synthesis method, we find that it is challenging to obtain the dimethylammonium bismuth sulfide intermediate product, and that Bi<sub>2</sub>S<sub>3</sub> with dimethylammonium iodide on the surface likely forms instead. The significant I-containing residues in this intermediate results in Cs<sub>3</sub>Bi<sub>2</sub>I<sub>9</sub> being preferentially formed in thin films instead of CsBiSCl<sub>2</sub>. Solid state synthesis without I present leads to phase impurities, consistent with the lowest-energy CsBiSCl<sub>2</sub> phase being metastable. Taking these experimental and

Received 00th January 20xx, Accepted 00th January 20xx

DOI: 10.1039/x0xx00000x

## Introduction

Developing solar absorbers that are simultaneously efficient, stable, comprised of nontoxic, earth-abundant elements, and can be produced cost-effectively has long been an elusive target of the broad thin film photovoltaics community. This effort was disrupted by the discovery that lead-halide perovskites (LHPs) can achieve effective optoelectronic properties (long diffusion lengths, high luminescence quantum yields, and low Urbach low-cost, low-temperature energies) using fabrication methods. This strongly contrasts with traditional semiconductors, such as crystalline silicon (c-Si) or III-V compounds.<sup>1-3</sup> Not only have LHPs now been realized in photovoltaics with similar power conversion efficiencies (PCEs) as industry-dominant c-Si solar cells (certified PCEs of 27.0% for LHP, and 27.8% for c-Si at present),4 LHPs have catalyzed the development of new classes of solar absorbers. These materials are termed 'perovskite-inspired', and include compounds that are structurally analogous (e.g., halide elpasolites or double perovskites),<sup>5</sup> chemically analogous (e.g., tin perovskites),<sup>6</sup> or electronically analogous (e.g., NaBiS<sub>2</sub>).<sup>7</sup> A key property sought for is defect tolerance, where low non-radiative recombination rates are achieved despite high defect concentrations through low capture coefficients of the most common point defects,

self-healing, or the formation of benign defect pairs.<sup>8,9</sup> There has especially been emphasis on heavy pnictogen-based compounds, namely Sb- and Bi-based materials,<sup>10–12</sup> which have stable valence *ns*<sup>2</sup> electrons that are believed to be conducive towards achieving defect tolerance.<sup>13</sup> Although these materials overcome the toxicity and stability limitations of LHPs, their performance thus far has been limited, with the majority of materials realized in photovoltaic devices having PCEs well below 10%.<sup>14–16</sup>

Remarkably, Huang et al. reported a PCE of 10.4% from solar cells based on CsBiSCl<sub>2</sub>.17 Surprisingly, this high PCE was achieved in the first report of this material in solar cells. A PCE of 10% is considered a threshold for a new photovoltaic material to hold promise for commercialisation. Indeed, looking back at the development of LHPs: although the first publication of this material in solar cells was reported by Miyasaka and co-workers in 2009,18 it was not until Snaith and co-workers reported a PCE exceeding 10% in 2012 19 that the field began to gravitate towards this material. 20-22 It is therefore significant that CsBiSCl<sub>2</sub> was reported to immediately achieve >10% PCE in the first publication on this material for solar cells. Furthermore, this material was claimed to be substantially more environmentally stable than LHPs, with the PCE maintaining 97% of the original value after storage for 150 days without encapsulation in ambient air. CsBiSCl<sub>2</sub> is also free from any toxic elements regulated by the Restriction of Hazardous Substances (RoHS) directive.<sup>23</sup> The bandgap of 2.0 eV for this material is close to the ideal value for indoor photovoltaics, 24,25 as well as X-ray detectors,26 and could also be well suited for solar water splitting.27

<sup>&</sup>lt;sup>a</sup> Inorganic Chemistry Laboratory, University of Oxford, South Parks Road, Oxford, OX1 3QR, United Kingdom. E-mail: <a href="mailto:robert.hoye@chem.ox.ac.uk">robert.hoye@chem.ox.ac.uk</a>

b. Department of Materials and Centre for Processable Electronics, Imperial College London, Exhibition Road, London, SW7 2AZ, United Kingdom

<sup>†</sup> These authors contributed equally: Eilidh L. Quinn, Hugh Lohan Supplementary Information available: Details of random structure searching calculations, structure analysis and compositional analysis. See DOI: 10.1039/x0xx00000x

This article is licensed under a Creative Commons Attribution 3.0 Unported Licence.

Open Access Article. Published on 28 2025. Downloaded on 04/11/25 22:34:50.

**ARTICLE** 

**Journal Name** 

However, the crystal structure of CsBiSCl<sub>2</sub> is not known, and the original report of CsBiSCl<sub>2</sub> solar cells did not use any refinement methods to fit the measured X-ray diffraction pattern with a proposed structure.<sup>17</sup> Understanding the structure of a material is critical. The crystal structure defines essential properties, including the stability, as well as the electronic structure, which in turn affects the bandgap and charge-carrier mobility (through the effective mass). Determining the structure is mandatory for performing atomistic simulations, including defect calculations, and determining the upper limit in efficiency of the material. Therefore, it is paramount to first understand the crystal structure of CsBiSCl<sub>2</sub> and verify the stoichiometry of the compound formed.

Huang et al. suggested that  $CsBiSCl_2$  adopts an n=1Dion-Jacobson perovskite structure, comprised of layers of BiS<sub>2</sub>Cl<sub>4</sub> corner-sharing units, with Cs<sup>+</sup> cations in between these layers (Fig. 1a, left).<sup>17</sup> However, there is no evidence for this structure. The general formula for the Dion-Jacobson homologous series is  $A'A_{n-1}Pb_nX_{3n+1}$  (A'=1+ or 2+ cation, A = 1+ cation, X = 1- anion). <sup>28</sup> Adapting this formula to the Cs-Bi-S-Cl quaternary system depicted in Fig. 1a left, where n=1, gives the stoichiometry CsBi(S,Cl)<sub>4</sub>, not CsBiSCl<sub>2</sub>. This CsBi(S,Cl)<sub>4</sub> stoichiometry cannot be achieved with the standard oxidation states for the cations (I for Cs, III for Bi) and anions (II for S, I for CI) without violating the rules of charge neutrality (details in Table S1, SI). If we take the structure as drawn in Fig. 1a left, then S:Cl should be 1:3, but this requires Bi to be in the IV oxidation state, which is unlikely given the stability of the 6s2 electron pair. Therefore, the suggestion that the polyhedra in CsBiSCl<sub>2</sub> form layers with a corner-sharing Dion-Jacobson structure is unfounded.

Alternative structures for CsBiSCl<sub>2</sub> may be more plausible. There have been studies into other I-III-VI-VII2 materials, with a particular focus on lead-free analogues of CH<sub>3</sub>NH<sub>3</sub>PbI<sub>3</sub>. In these materials, the Pb2+ cation is replaced with trivalent Sb3+ or Bi3+ and one I<sup>-</sup> anion is replaced with a chalcogenide anion (S<sup>2-</sup> or Se<sup>2-</sup>) to maintain charge neutrality, forming a split-anion perovskite.<sup>29</sup> Films of CH<sub>3</sub>NH<sub>3</sub>SbSI<sub>2</sub> have been reported with the suggestion that the phase adopts a near-ideal perovskite structure based on a near-ideal calculated Goldschmidt tolerance factor of t = 0.99.<sup>30</sup> The Bi analogue, CH<sub>3</sub>NH<sub>3</sub>BiSl<sub>2</sub>, has also been reported, although it was proposed that this material preferentially adopts an orthorhombic or rhombohedral lattice as t < 0.9.31 However, further experimental and density functional theory (DFT) studies found no evidence for the formation of I-III-VI-VII<sub>2</sub> perovskites, instead showing that the formation of the ternary  $A_3M_2X_9$  phase, along with binary chalcogenides and halides, is more energetically favourable.<sup>32</sup>

Quarta et al. attempted to prepare nanocrystals of CsBiSCl<sub>2</sub>.33 They proposed a cubic perovskite structure for this material (Fig. 1a, right) by using CrystaLLM, which is based on an autoregressive large language model, trained on millions of crystallographic information files.34 However, their synthesis attempts were unsuccessful, and CsBiSCl<sub>2</sub> with a perovskite

phase was not obtained experimentally, instead forming in mixture of Cs<sub>3</sub>BiCl<sub>6</sub>, Cs<sub>3</sub>Bi<sub>2</sub>Cl<sub>9</sub> and Bi<sub>2</sub>S<sub>3</sub>. Another possibility is the UFeS<sub>3</sub> structure type. This has been reported for both AgBiSCl<sub>2</sub> nanocrystals and polycrystalline powders of CuBiSCl<sub>2</sub>. <sup>35,36</sup> This is a layered structure with alternating slabs of [AS<sub>2</sub>Cl<sub>4</sub>]<sup>7-</sup> distorted octahedra, and [BiS<sub>2</sub>Cl<sub>6</sub>]<sup>7-</sup> bi-augmented triangular prisms. However, this structure has not yet been investigated as a possibility for the CsBiSCl<sub>2</sub> phase.

Already, several review papers have cited CsBiSCl2 as an important prospect in lead-free photovoltaics due to the reportedly high performance and excellent cell stability.9,37-40 However, such claims are, as-yet, premature without understanding what the structure adopted is, and whether the reported thin film synthesis route<sup>17</sup> is a valid approach to obtain this structure with the intended stoichiometry. It is critical to address these questions before the photovoltaics field dedicates more effort into this material. 19-23

In this work, we first adopt a systematic global structure search to determine the ground state structure of CsBiSCl2. The approach is ab-initio Random Structure Searching (AiRSS), coupled with a bespoke Ephemeral Data Derived Potential (EDDP) to determine whether (meta-)stable CsBiSCl₂ structures exist and if previously-proposed perovskite structures are energetically accessible. Next, we repeat the synthesis method reported by Huang et al. for thin films. We examine the composition, and phases present in the reaction intermediate and final thin film product through energy-dispersive X-ray spectroscopy (EDX), as well as Pawley refinement of the measured diffraction patterns with possible structures for CsBiSCl<sub>2</sub> and phase impurities. We use Fourier transform infrared spectroscopy (FTIR) to identify molecular species present, along with UV-visible (UV-vis) spectrophotometry to identify the absorption profiles of the thin film products formed. Given that the reported thin film synthesis route involves the use of HI, we compare with a solid-state melt synthesis approach that only uses the elements present in the target material, i.e., using CsCl, BiCl<sub>3</sub> and Bi<sub>2</sub>S<sub>3</sub> precursors. This work provides a thorough evaluation of the potential of CsBiSCl2 as a solar absorber, and whether the wider photovoltaics field should dedicate further effort into this novel lead-free material.

# Results and discussion

## Identifying the Lowest-Energy Structure of CsBiSCl<sub>2</sub>

The AiRSS method involves iteratively generating 'chemically sensible' trial structures, relaxing them using an energy/force calculator, recording the result in a ranked database of energies, and repeating until some stopping criteria have been reached, e.g., rediscovery of the same lowest energy structures multiple times (refer to Experimental section). Interesting structures, typically those within 100 meV/atom of the thermodynamic convex hull, can then be refined using precise density functional theory (DFT) settings.

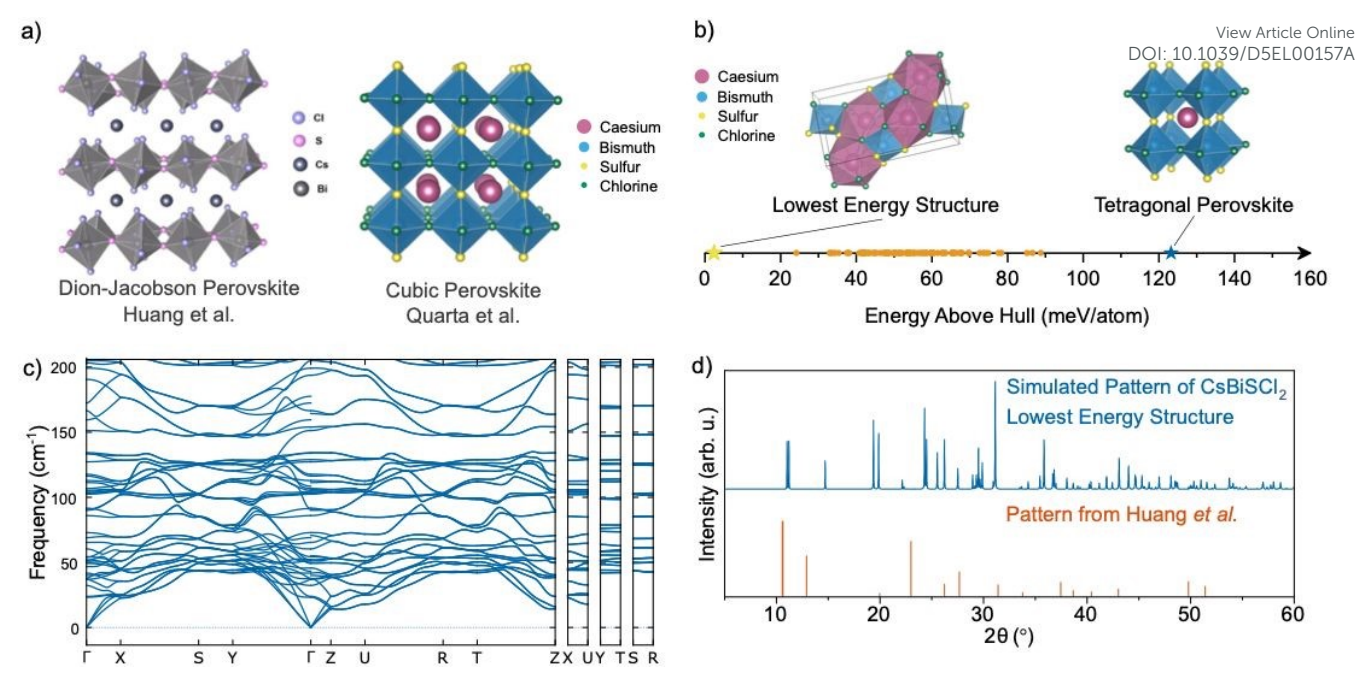


Figure 1. Structure of CsBiSCl<sub>2</sub> (a) Proposed crystal structure of CsBiSCl<sub>2</sub> by Huang et al. <sup>17</sup> and Quarta et al. <sup>33</sup> Illustration of structure proposed Huang et al. reprinted with permission from J. Huang et al., J. Phys. Chem. Lett., 2024, **15**, 3383–3389, Cubic perovskite structure prepared from the information provided in Ref. 33. (b) Energy above the Cs-Bi-S-Cl convex hull of CsBiSCl<sub>2</sub> structures selected for DFT refinalization. Shown are the lowest energy structure (yellow star), tetragonal perovskite structure (blue star), and remaining (csBiSCl<sub>2</sub> structures within 70 meV/atom of the hull (orange circles). (c) Phonon dispersion curve of the lowest-energy CsBiSCl<sub>2</sub> structure found from AiRSS. Lack of imaginary modes (i.e., no negative frequencies) demonstrates the dynamic stability of this structure. (d) Comparison of the simulated powder X-ray diffraction (PXRO) pattern for the lowest energy Pnma structure and the CsBiSCl<sub>2</sub> PXRD pattern reported by Huang et al. <sup>17</sup> Comparison with tetragonal perovskite reference pattern shown in Fig. S6, SI.

For relatively simple materials (unaries, binaries) with small unit cells, it is tractable to carry out all geometry relaxations using DFT. However, for compositionally complex materials where the search space is large, and/or those where a large unit cell is expected, traditional structure search soon becomes prohibitively expensive. Accelerating the structure search could be achieved using machine learning interatomic potentials (MLIPs). MLIPs can be classified as *foundation* or *bespoke* models, the former being trained on databases of diverse training data (e.g., Materials Project's MPtrj <sup>41–43</sup>) with the goal of being applicable to arbitrary chemical systems, while the latter are trained on much smaller and narrower datasets, usually prepared by a single researcher, with a specific system in mind (e.g. Cs-Bi-S-CI). Bespoke models are not transferable to arbitrary systems.

This article is licensed under a Creative Commons Attribution 3.0 Unported Licence

Open Access Article. Published on 28 2025. Downloaded on 04/11/25 22:34:50.

We initially attempted to use the foundation model MatterSim<sup>44</sup> to drive structural relaxations, but found it to have limited output structural diversity within the Cs-Bi-S-Cl system, as detailed in Supplementary Note S1. We therefore trained a bespoke EDDP tailored to predicting the energy of CsBiSCl<sub>2</sub> structures. EDDPs are formulated specifically for random structure searching and, by design, avoid common pitfalls associated with modelling far-from-equilibrium structures using MLIPs.<sup>45</sup> To train the EDDP, the energies of 51 212 structures in the Cs-Bi-S-Cl space were calculated using DFT (PBEsol-D4). While the majority of structures were of the CsBiSCl<sub>2</sub> stoichiometry, the dataset also included all low-energy Materials Project structures within the Cs-Bi-S-Cl space, optimised perovskite CsBiSCl<sub>2</sub> structures, as well as a set of randomly generated unary, binary and ternary structures to

improve the model fit. Crucially, this dataset included structures spanning the entire search space, from high-energy to nearequilibrium ones. The as-trained EDDP had final training root mean squared error (RMSE) and mean absolute error (MAE) of 48.16 meV and 30.98 meV, while the testing RMSE and MAE were 235.94 meV and 42.40 meV.

The testing RMSE was raised by a single outlier with an error of > 15 eV. While the global RMSE/MAE is quite high, this is mostly increased by non-stoichiometric and far-from-hull structures included in the dataset. The testing RMSE/MAE for CsBiSCl<sub>2</sub> structures within 1 eV of the hull are significantly improved at 22.7 meV/atom and 13.8 meV/atom respectively (Fig. S1, SI). Full details may be found in the Experimental section.

Using the as-trained EDDP, 92 770 CuBiSCl<sub>2</sub> structures with 2–10 formula units were generated and relaxed to their local minima. Of these, 3732 structures within 70 meV/atom of the convex hull were selected, and similar structures unified using a similarity threshold of 0.01, resulting in 118 unique low energy structures, after removal of one unphysical 'low-energy' structure (Fig. S2, SI). The lowest energy structure was rediscovered eleven times, and is a four formula unit *Pnma* structure (Fig 1b). This structure was significantly lower in energy (by 28.2 meV/atom) than the next lowest-energy structure.

In an attempt to catch any low energy structures missed by standard AiRSS, 25 ps molecular dynamics (MD) simulations near the melting point of the *Pnma* structure were carried out for the top 10 000 structures (2778 after unification) using the

ARTICLE Journal Name

bespoke MLIP and supercells of at least 40 atoms (so called 'hot-AiRSS' method). He while this reduced the number of unique structures after symmetrization and unification by 14% and resulted in the rediscovery of the *Pnma* structure another eight times; no lower energy structures were found. This supports the conclusion that the low-energy *Pnma* structure is dynamically stable. The structural density of states was flattened and broadened by this process, suggesting melting occurred in the far-from-hull regions (Fig. S3, SI).

The 118 unique low-energy structures, Materials Project (MP) near-the-hull structures, and the previously-proposed perovskite structures were selected for relaxation using precise DFT settings and more accurate Hamiltonian (r²SCAN-D3(BJ)+SOC). This high level of theory was chosen as the distance from the hull was within the margin of error set by our previous GGA/high-throughput DFT dataset. We found the lowest-energy *Pnma* structure predicted using EDDP-AiRSS remains the lowest energy CsBiSCl<sub>2</sub> structure in the refinalized DFT dataset and sits just 2.4 meV/atom above the Cs-Bi-S-Cl convex hull (Table S2, SI). This implies it is an energetically accessible structure, but no stable CsBiSCl<sub>2</sub> structures (*i.e.*, directly on the convex hull of the Cs-Bi-S-Cl system) were discovered.

To confirm the dynamic stability of the low-energy Pnma structure, a tight relaxation and subsequent harmonic phonon dispersion curve was calculated (Fig 1c). We found that, despite the presence of low-lying optical modes near the Z point, the structure is dynamically stable with no imaginary modes present. Due to its proximity to the convex hull and its dynamic stability, the low-energy Pnma structure is a plausible metastable synthetic target. We estimate this structure has a bandgap of >1.9 eV (Fig. S4, SI). Whilst this bandgap is suitable for top-cells in tandem photovoltaics, and for indoor photovoltaics, we note that using a meta-GGA functional would typically underestimate the bandgap, and there is a risk that the actual bandgap of the low-energy Pnma compound is substantially above 2 eV, making it not well suited for these applications. Furthermore, visual comparison of the simulated powder X-ray diffraction (PXRD) pattern of the low-energy Pnma structure with the PXRD pattern reported by Huang et al. for CsBiSCl<sub>2</sub> showed very little similarity (Fig. 1d).

Interestingly, we found the previously-proposed cubic perovskite structure to be energetically implausible. Upon relaxation, the cubic perovskite structure undergoes a second-order Jahn-Teller distortion, resulting in a tetragonal structure where bismuth atoms are off-centred in their S²-/Cl-octahedra. This tetragonal perovskite has a large energy above hull of 123 meV/atom (Table S2, SI). In addition, visual comparison between the pattern reported by Huang *et al.* and the simulated pattern of the tetragonal structures shows little similarity (Fig. S6, SI). As such, we do not expect perovskite-structured CsBiSCl<sub>2</sub> to be experimentally accessible using standard synthetic approaches.

 $\label{localization} \mbox{ View Article Online } \mbox{ Investigation of the 'DMABiS}_2' \mbox{ Intermediate} : 10.1039/D5EL00157A$ 

The solution synthesis method reported by Huang *et al.* involved using CsCl and dimethylammonium bismuth sulfide (DMABiS<sub>2</sub>) precursors, dissolved in a mixture of *N,N*-dimethylformamide (DMF) and dimethyl sulfoxide (DMSO), from which thin films of CsBiSCl<sub>2</sub> were spin coated.<sup>17</sup> DMABiS<sub>2</sub> rather than Bi<sub>2</sub>S<sub>3</sub> was used as the Bi and S precursor because it was suggested that this offers greater solubility in polar organic solvents.

The synthetic route to this 'DMABiS<sub>2</sub>' intermediate involves introduction of the dimethylammonium cation (DMA+) to Bi<sub>2</sub>S<sub>3</sub> through in-situ acid hydrolysis of the DMF amide bond, catalyzed by HI (Fig. 2a). The generation of DMA+ cations through DMF hydrolysis has been previously applied to the synthesis of Cs<sub>1-x</sub>DMA<sub>x</sub>PbI<sub>3</sub> hybrid perovskites.<sup>47</sup> There was no suggested structure for the previously unreported DMABiS2 intermediate. Bi<sub>2</sub>S<sub>3</sub> has a 2D layered (lamellar) structure with layers connected by weak van der Waals interactions, with an interlayer spacing of 0.23 nm.<sup>48,49</sup> Insertion of cations between the layers has been used to prepare intercalation compounds of Bi<sub>2</sub>S<sub>3</sub> that have potential applications as battery materials.<sup>50,51</sup> It may be the case that DMABiS2 is an intercalation product, with DMA+ cations between the layers of Bi<sub>2</sub>S<sub>3</sub>. If this were the case, it is to be expected that PXRD peaks assigned to Bi<sub>2</sub>S<sub>3</sub> should shift to lower  $2\theta$  values.

To synthesize the DMABiS $_2$  intermediate, we mixed 1.8 g Bi $_2$ S $_3$  powder (3.5 mmol) with 3 mL DMF solvent in an N $_2$ -filled glovebox, according to the method from Huang *et al*. We found that full dissolution of Bi $_2$ S $_3$  did not occur, nor during the addition of 2.5 mL HI dropwise to this mixture. After mixing for 4 h at 500 rpm, we used Büchner filtration of the mixture inside a fume hood, obtaining a dark brown intermediate product, which is consistent with the report from Huang *et al*. <sup>17</sup> But we also obtained an orange precipitate from the filtrate after washing with ethanol. This was not reported in the original synthesis. Fig. 2b shows photographs of both the dark brown product powder and the orange precipitate recovered from the filtrate.

We measured the PXRD pattern of the dark brown product and orange powder from the filtrate, and analyzed through Pawley fitting (Fig. 2c). This refinement method fits the peak positions according to the structure files input, but numerically fits the peak intensities. Pawley fitting is therefore suitable for obtaining lattice parameters and identifying whether the measured pattern is accounted for by the proposed structures, but does not solve the atomic coordinates. This is an appropriate step for determining the phase purity of the powder before performing Rietveld refinement to obtain atomic coordinates, ideally from a phase-pure sample that does not have preferred orientation.

Given that the structure of DMABiS<sub>2</sub> has not been solved, we first extracted the reported XRD peaks of this intermediate from

Solar Accepted Manuscrip

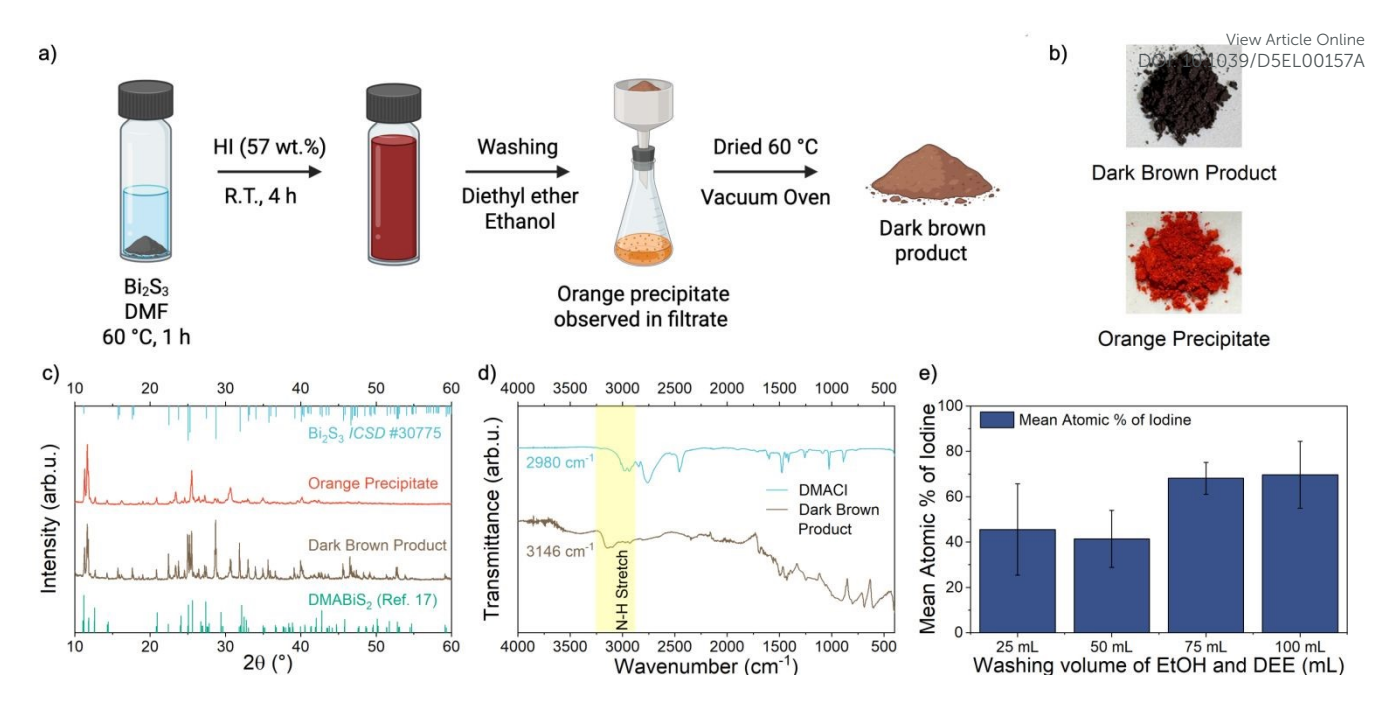


Figure 2. Preparation of DMABiS<sub>2</sub> Intermediate. (a) Illustration of the synthesis procedure for preparation of the DMABiS<sub>2</sub> intermediate. Created in BioRender. Quinn, E. (2025) https://BioRender.com/xo6o9y9 (b) Images of the dark brown product powder and the orange precipitate observed in the filtrate during the washing stage. (c) PXRD pattern of synthesized DMABiS<sub>2</sub> material. The light blue bars indicate the reference patterns of Bi<sub>2</sub>S<sub>3</sub> (ICSD #30775), while the light green bars represent the reported pattern by Huang *et al.* for their claimed DMABiS<sub>2</sub> intermediate. (d) Infrared spectra of the dark brown powder and DMACI reference material. The peaks assigned to the ammonium N-H stretch are highlighted. The increase in peak wavenumber for the dark brown powder sample is attributed to the reduction in electronegativity of the environment leading to stronger N-H bonds. (e) The effect of solvent washing volume on the mean atomic percentage of iodine from EDS measurements of dark brown product powders. The error of atomic percentage is calculated using procedure described in Fig. S12, S1.

Ref. 17, and visually compared against the PXRD pattern for our dark brown product. As shown in Fig. 2c, there is a good match to all of the reference DMABiS $_2$  peaks, especially the strong peaks at 12° 2 $\theta$ , which were claimed by Huang *et al.* to "confirm" the formation of DMABiS $_2$ .<sup>17</sup> There are, however, some peaks present in our dark brown product not present in the previously-reported pattern for DMABiS $_2$ , suggesting that there are other phases present, or that we do not have a DMABiS $_2$  intercalation product.

We tested the hypothesis that the dark brown product is Bi<sub>2</sub>S<sub>3</sub>, performing Pawley fitting (Fig. S7a, SI) using the structure file from the Inorganic Crystal Structure Database (ICSD), collection code: 30775. As shown in Fig. 2a, there is a good match, with a goodness of fit (GoF) of 3.13. However, residuals are present, notably at 12°, 20°, and 30°  $2\theta$ . We therefore tested the hypothesis that а second phase was present: dimethylammonium iodide (DMAI). This improved the refinement (Fig. S7b, SI), with a goodness of fit of 2.99, although the key residuals at 12°, 20°, and 30° 2 $\theta$  are still present. Therefore, we propose that the dark brown product we prepared is likely to contain two separate phases: Bi<sub>2</sub>S<sub>3</sub> and DMAI, and possibly with a third unidentified phase. None of the peaks assigned to the  $Bi_2S_3$  phase show a shift in  $2\theta$  position compared to the reference pattern. We therefore conclude that it is unlikely that there is an intercalation product.

SEM and EDX measurements were performed to aid the characterization of the prepared material. We observed two distinct phases: larger particles with a layered surface, and

smaller particles dispersed across the surface of the larger particles. EDX analysis (Fig. S9 and Table S3, SI) suggested that the layered material was Bi<sub>2</sub>S<sub>3</sub>, with I impurities. The smaller particles contained a significant proportion of I and higher levels of N, suggesting that these smaller particles are likely to be primarily DMAI. This provides further evidence that no uniform DMABiS<sub>2</sub> phase was synthesized, but that the reported synthetic route prepares Bi<sub>2</sub>S<sub>3</sub> with DMAI contamination, along with I residues throughout the sample. We considered the possibility that BiSI may be present, however, Pawley refinement to BiSI structure file (ICSD Collection Code: 133376) revealed a poor match to this phase with a GoF of 4.79 (Fig. S9, SI). This allowed us to discount the presence of a BiSI phase.

Infrared (IR) spectroscopy data confirms the presence of an ammonium species in the dark brown product powder. Fig. 2d shows the IR spectrum of the material alongside the IR spectrum of reference DMACI material. The peak at 3146 cm<sup>-1</sup> is assigned to the N-H stretch of the DMA<sup>+</sup> cation. This is at a higher wavenumber than the corresponding N-H stretch peak in the DMACI reference (2980 cm<sup>-1</sup>). We attribute this observation to the reduction in electronegativity of the environment surrounding the DMA<sup>+</sup> cation, since replacing CI with I in DMAX would increase the electron density in the N-H bonds, making them stronger and oscillate faster.

We also analyzed the orange precipitate obtained from the filtrate. Its PXRD pattern is broadly similar to the pattern of the dark brown product, but significantly less crystalline, especially

This article is licensed under a Creative Commons Attribution 3.0 Unported Licence.

Open Access Article. Published on 28 2025. Downloaded on 04/11/25 22:34:50.

ARTICLE Journal Name

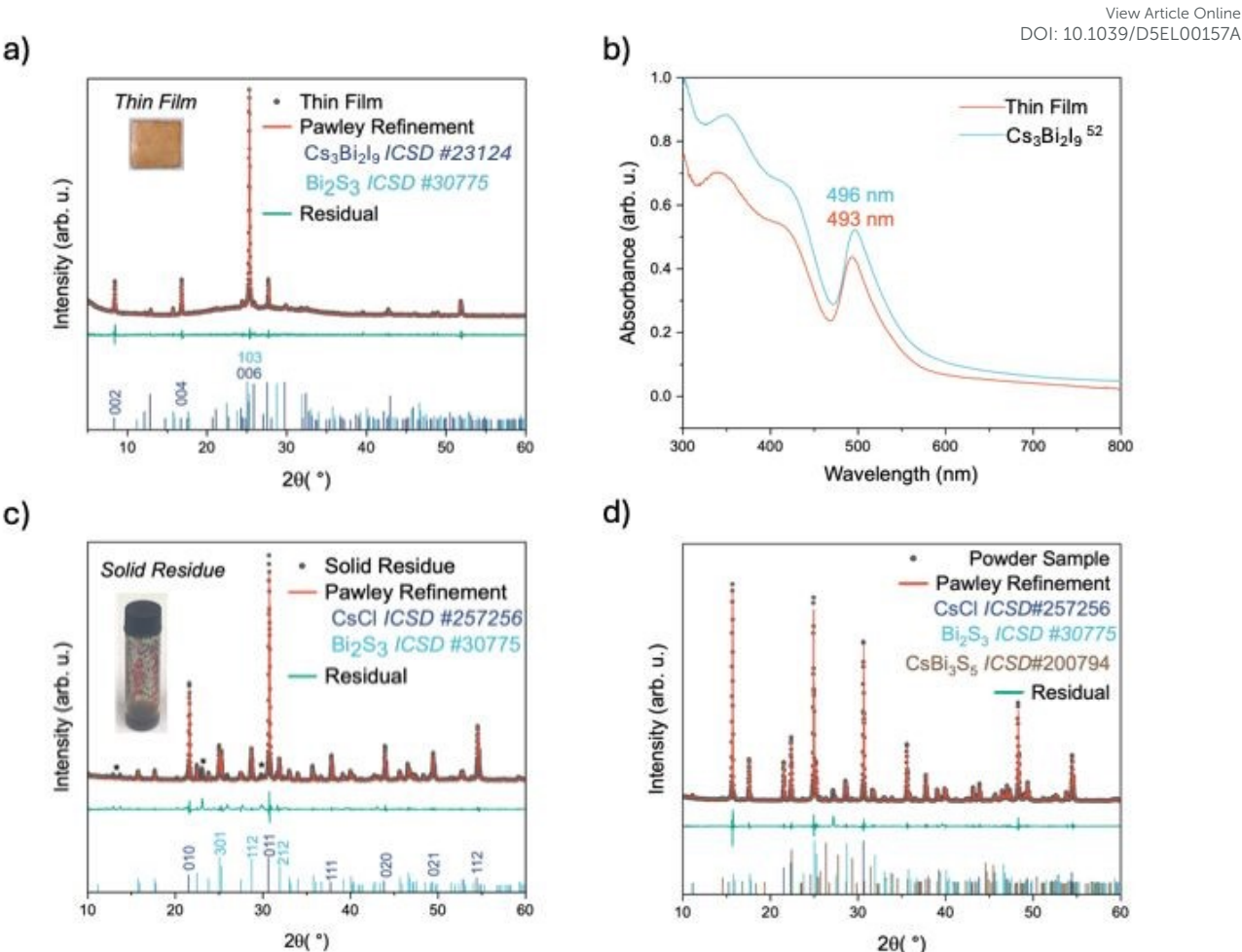


Figure 3. Challenges with CsBiSCl<sub>2</sub> synthesis (a) PXRD pattern of thin films synthesized according to Huang *et al.* (solid circles), with the corresponding Pawley refinement to  $Cs_3Bi_2l_9$  and  $B_{12}S_3$  (red line); Rwp = 9.1874 GoF = 1.2124. Inset: Photograph of the as-prepared thin film on 1.4 cm² glass. (b) UV-Vis absorption spectrum of prepared thin films and  $Cs_3Bi_2l_9$  reference spectrum,  $s^{52}$  with the characteristic  $Cs_3Bi_2l_9$  excitonic peaks labelled. (c) PXRD pattern of solid residue from precursor solution from the attempted synthesis of CsBiSCl<sub>2</sub> (solid circles), with the corresponding Pawley refinement to  $Bi_2S_3$  and CsCl (red line); Rwp = 12.9970 GoF = 2.1417, unidentified peaks are labelled by \*. Inset: Photograph of the solid residue in a glass vial. (d) PXRD pattern of material from attempted solid-state synthesis of CsBiSCl<sub>2</sub> (solid circles), with the corresponding Pawley refinement to  $CsCl_3Bi_2S_3$ , and  $CsBi_3S_5$  (red line); Rwp = 10.9693, Rwp =

at higher  $2\theta$  values. We therefore concluded that this orange precipitate was not the desired DMABiS<sub>2</sub> intermediate material. IR measurements of the orange precipitate (Fig. S10, SI) showed no distinct functional group features, providing further support that this precipitate was not the desired ammonium bismuth sulfide intermediate.

A significant limitation of this method for preparing the intermediate product is the high I contamination from DMAI. In an attempt to reduce this contamination, we increased the volumes of diethyl ether (DEE) and ethanol (EtOH) used to wash the powders from 25 mL to 50 mL, 75 mL, and 100 mL. Fig. 2e shows that despite increased washing volumes, iodine contamination was still significant, and no reduction in I wt.% was observed from EDX of the dark brown powders. This may be because DMAI is strongly bound to the surface of Bi<sub>2</sub>S<sub>3</sub>, and cannot be removed through washing in polar solvents.

#### Challenges with CsBiSCl<sub>2</sub> Synthesis

We attempted to prepare CsBiSCl2 thin films from our intermediate dark brown product (details in Experimental). Fig. 3a shows the XRD patterns of the thin films obtained. Pawley analysis showed that the final film was a mixture of phases: Bi<sub>2</sub>S<sub>3</sub> and Cs<sub>3</sub>Bi<sub>2</sub>I<sub>9</sub>. The stronger intensity of the peaks assigned to Cs<sub>3</sub>Bi<sub>2</sub>I<sub>9</sub> suggest that this is the main phase. Data from UV-visible spectrophotometry (UV-vis) support this. Fig. 3b shows the UV-Vis absorption spectrum of the films prepared alongside the reported absorption spectrum of Cs<sub>3</sub>Bi<sub>2</sub>I<sub>9</sub>.<sup>52</sup> Both exhibit a distinct absorption onset peak centred at 493 nm wavelength. This peak is characteristic of Cs<sub>3</sub>Bi<sub>2</sub>I<sub>9</sub>, and has been attributed to the first excitonic peak.<sup>53</sup> Furthermore, the fine structure of the absorption spectrum aligns with previously reported broader peaks at 426 nm, 359 nm, and 310 nm, associated with the higher-order excitonic states. This corroborates that the thin films were primarily Cs<sub>3</sub>Bi<sub>2</sub>I<sub>9</sub>, as opposed to CsBiSCl<sub>2</sub>. Iodine contamination of the intermediate materials has significant consequences for the preparation of the final thin films, resulting in preferential formation of iodide phases over the desired CsBiSCl2 product. Additionally, Pawley refinement of the PXRD patterns suggests no incorporation of Cl-based phases

Solar Accepted Manus

into the thin films, since the peak positions match those of the reference pattern for  $Cs_3Bi_2l_9$ . This is supported by EDX observations of prepared films (Fig. S11 and Table S4, SI).

Another problem with this solution synthesis approach is that the solid reagents did not completely dissolve in the DMF/DMSO mixture. The residual solid was collected, dried in a vacuum oven at 60 °C overnight, and analyzed by PXRD. Pawley refinement of this solid confirms that this powder is a mixture of Bi<sub>2</sub>S<sub>3</sub> and CsCl (Fig 3c).<sup>54–56</sup> This is unsurprising given the poor solubility of CsCl in both DMF and DMSO due to its large lattice energy,<sup>57</sup> and provides further support for the dark brown intermediate product being primarily Bi<sub>2</sub>S<sub>3</sub> with DMAI attached.

#### **Alternative Solid-State Synthesis Route**

Given the challenges due to I contamination, we attempted solid state synthesis of CsBiSCl<sub>2</sub> by sealing ground and pelletized CsCl, Bi<sub>2</sub>S<sub>3</sub>, and BiCl<sub>3</sub> in quartz ampoules under vacuum. Due to the low boiling point of BiCl<sub>3</sub>, a synthesis temperature of 250 °C was chosen. While this is relatively low, there are reports of successful synthesis of ternary BiSCl under similar conditions.<sup>58</sup>

No single-phase powders were obtained from this solid-state synthesis. Rietveld refinement (Fig. 3d) of the powders revealed a mixture of binary (CsCl, Bi<sub>2</sub>S<sub>3</sub>) and ternary (Bi<sub>3</sub>CsS<sub>5</sub>) phases (goodness of fit of 1.74). As shown in Table S2, SI, all of these phases are on the convex hull of the Cs-Bi-S-Cl system. No peaks corresponding to a CsBiSCl<sub>2</sub> perovskite phase were observed in the powders. A lower temperature synthesis was also run at 175 °C, but this contained binaries and ternaries, as well as some unidentified products. This shows that for low-temperature solid-state synthesis, binary and ternary phases form preferentially over the desired quaternary phase. Thus, although the lowest-energy CsBiSCl<sub>2</sub> phase is 2.4 meV/atom above the DFT convex hull, it still proves challenging to access this phase.

# **Conclusions**

In this work, we investigated the quaternary CsBiSCl<sub>2</sub> system. Through a global structure search, we found that it is energetically unfavorable for this compound to adopt a regular perovskite structure, in contrast to previous assumptions. Instead, we identified an orthorhombic structure within 2.4 meV/atom of the thermodynamic convex hull, which is dynamically stable, implying it is a plausibly accessible metastable target. We repeated the thin film synthesis reported by Huang et al., demonstrating that the reported DMABiS2 intermediate is not a uniform phase but rather DMAI bound to the surface of Bi<sub>2</sub>S<sub>3</sub>. We attempted to prepare thin films, but were unable to prepare any phase pure films of CsBiSCl2, instead primarily obtaining films of Cs<sub>3</sub>Bi<sub>2</sub>I<sub>9</sub> due to I contamination in the intermediate product that is difficult to remove through solvent washing. Finally, we showed through an I-free solid-state synthesis that it is challenging to obtain CsBiSCl<sub>2</sub>, instead forming phases that are on the convex had lower therefore find that the 10% PCE claim made in the convex had lower is spurious, and recommend directing efforts away from this material. We suggest that focus should be shifted toward known Bi-based quaternary mixed-metal chalcohalides, such as AgBiSCl<sub>2</sub> and CuBiSCl<sub>2</sub>, <sup>35,36</sup> wherein the structure of the material has been solved and there remains significant research scope surrounding the synthesis of these materials and optimization of device performance.

# **Experimental**

#### **Calculations**

Structure search was carried out using the AiRSS method, with structural relaxations completed using an ephemeral data derived potential (EDDP), i.e., a small bespoke MLIP iteratively trained on single point DFT energies of structures in the Cs-Bi-S-Cl space.

A typical AiRSS workflow involves four steps:

- 1) Randomly generating a 'sensible' Cs-Bi-S-Cl structure using simple rules derived from chemical intuition, e.g., enforcing a minimum separation between atoms, fixed stoichiometry;
- 2) Use a (DFT) energy/forces calculator to optimize this structure until forces on atoms are below a desired threshold; 3) Add structure and to a ranked database of energies.

Steps 1-3 are repeated until some stopping criteria is reached, such as when the lowest energy structure has been rediscovered multiple times. At this point a subset of 'interesting' structures, usually those within 100 meV/atom of the convex hull, are refined using precise DFT settings.

### Training of MLIP

The EDDP suite consists of four packages; 'airss', 'ddp', 'repose', and 'nn'.<sup>46,59,60</sup> These packages are used for random structure generation/search, training of (E)DDPs, structural optimisation, and implementing neural nets respectively.

An EDDP was iteratively trained using the `chain` script and an initial dataset of 10 000 random  $\mathsf{CsBiSCl_2}$  structures generated using AiRSS utility `buildcell`,^6¹ as well as a 'marker' dataset of all <40 atom structures in the Cs-Bi-S-Cl phase space within 20 meV of the convex hull available on Materials Project.^41,62,6³ Marker structures were randomly shaken 50 times each with an amplitude of 0.04 Å. DFT single-point energies were calculated for each structure in the training set using CASTEP 24.1  $^{64}$  and the high-throughput QC5 ultrasoft pseudopotential set with a cut-off energy of 425 eV, a minimum Monkhorst-Pack grid density of 0.05 Å-¹, and a fine grid scale of 2. The PBEsol  $^{65}$  functional with D4  $^{66}$  dispersion correction was used.

Approximately 256 DDPs were trained on this dataset using the ddp utility 'forge' trained and of these a subset were selected and cast into a weighted ensemble of DDPs (EDDP) by 'flock'. DDPs were trained using up to 3-body terms and a cutoff of 8.0

This article is licensed under a Creative Commons Attribution 3.0 Unported Licence.

Open Access Article. Published on 28 2025. Downloaded on 04/11/25 22:34:50.

**ARTICLE** Journal Name

Å, with a polynomial order of up to 16 for 2-body and up to 4 for 3-body terms, resulting in a feature vector with a length of 435. This was passed through a 5 node neural net and finally to the output layer.

Training, validation, and testing data was split in a ratio of 80:10:10. Using this EDDP and 'repose', 2000 random AiRSS structures were relaxed to their local minima. DFT total energies were calculated for these structures, added to the dataset, and used to train an improved EDDP. This iterative process was repeated a total of 5 times. To improve the performance of the MLIP, the training dataset was enriched with EDDP relaxed structures from the wider Cs-Bi-S-Cl space, as well as high and low density structures, resulting in a final dataset of 51,212 structures.

For the final MLIP, 213 DDPs were trained and 42 were selected and cast into an EDDP. To run the EDDP suite in a massively parallel way, the batch queuing utility 'DDP-batch' was utilised.<sup>67</sup> Random structure search was carried out using the as trained EDDP and 'repose', a structural optimiser native to the EDDP suite. This trained MLIP, training dataset, and the 'buildcell'/AiRSS input files used to generate it are available in the raw data repository. A total of 92 770 relaxations were carried out. Rediscovery rates were assessed by merging similar structures using the unite functionality of the 'cryan' tool in the 'airss' package, which compares unit cell volumes and interatomic distances within compared structures are within a specified threshold, e.g., 1%.

# **Refinalization of Low Energy Structures**

Structures selected for refinalisation included the 118 unique low-energy structures found via random structure search, 36 MP near-the-hull structures, and proposed perovskite structure. Materials project structures included all Cs-Bi-S-Cl structures within 20 meV/atom of the r2SCAN68 derived hull, which were also fewer than 50 atoms. Structures were relaxed using r2SCAN-D3(BJ)+SOC,  $^{68,69} as$  implemented in VASP 6.5.0  $^{70,71}$ and the accurate PAW PBE 'potpaw.64' pseudopotential set  $^{72}$ with semicore Cs s & p states treated as valence electrons. A basis set cutoff 450 eV was used, as well as a k-spacing of 0.25 Å-1 for insulators and 0.15 Å-1 for known metallic structures from Materials Project. Note, due to differences in definition, VASP grid spacings differ by a factor of  $2\pi$  to the equivalent CASTEP grid spacing. The 'kgrid' 73utility was used for adjusting the kpoint sampling density. Structures were optimised using the conjugate-gradient algorithm (IBRION=2) until forces on each atom were <0.03 eV/Å, and those near the hull (<30 meV/atom) were further optimised with a tighter force convergence criterion of <0.01 eV/Å.

#### Dynamic Stability of Low-Energy CsBiSCl<sub>2</sub> Structure

The low-energy Pnma structure was symmetrized using 'phonopy',74,75 further optimized until forces on each atom were <5e<sup>-3</sup> eV/Å. The orthorhombic primitive cell had dimensions of 9.45×4.13×16.08  $\text{Å}^3$  and a 4×8×2  $\Gamma$ -centered **k**- point grid was used during relaxation. 2×4×1 supercells and a commensurate  $2\times2\times2$  **k**-point grid were 1७३६४ / फिक्र- े पिर्वार displacements with a displacement amplitude of 0.01 Å. Born effective charges were extracted from a finite differences (IBRION=6) run on the primitive and used to estimate TO-LO splitting.

#### **Materials**

All chemicals were used as received without any further purification. Bismuth sulfide (Bi<sub>2</sub>S<sub>3</sub>, 99%), dimethyl sulfoxide (DMSO, ≥99.9%), hydroiodic acid (HI, 57 wt.%, 99.95%), ethanol (≥99.8%), and diethyl ether (≥99.8%) were purchased from Sigma-Aldrich. Cesium chloride (CsCl, 99.999%), bismuth chloride (BiCl<sub>3</sub>, 97%) and N,N-dimethylformamide (DMF, anhydrous, 99.9%) were purchased from ThermoFisher Scientific.

#### Preparation of DMABiS<sub>2</sub> Intermediate

 $1.80~g~Bi_2S_3$  and 3 mL DMF were stirred at 60 °C for 1 h. 2.5~mLHI was added dropwise and the suspension was stirred for 4 h. The suspension was filtered via Büchner filtration and washed with diethyl ether and ethanol. The resulting powder was dried in a vacuum oven overnight at 60 °C.

#### Attempted Synthesis of CsBiSCl<sub>2</sub> Thin Films

All steps, apart from substrate cleaning, were carried out inside N<sub>2</sub>-filled glovebox.

0.16 g of the dark brown intermediate product and 0.34 g CsCl were mixed in DMF/DMSO (9:1) and stirred at room temperature for 2 h. The suspension was allowed to settle for 24 h before the liquid phase was filtered with a 0.2 μm PTFE filter. A 1.2 cm × 1.2 cm substrate was cleaned by ultrasonication in acetone for 15 min, followed by isopropanol for 15 min. After cleaning, the substrates were blown dry with N2, followed by UV-ozone treatment (NanoBioAnalytics UV Ozone Cleaner UVC-1014) for 20 min. 40 µL of the filtered solution was spread onto the substrate followed by spinning at 1000 rpm for 10 s and 4000 rpm for 30 s. The deposited film was annealed at 220 °C for 1 h 20 min.

#### Attempted Synthesis of CsBiSCl<sub>2</sub> Powders

Polycrystalline samples of 'CsBiSCl2' were prepared by a solid-state reaction. In an N2-filled glovebox, BiCl3, Bi2S3, and CsCl were weighed and wet ground in acetone for 30 mins. 0.65 g aliquots were then pressed into 12 mm pellets by applying 9 ton. Pellets were sealed in 7 mm internal diameter quartz ampoules with a final length of 4 cm under a vacuum of 5×10-2 mbar. Pellets were submerged in liquid nitrogen during sealing. The ampoule pellet was heated directly using a torch before synthesis in a fume hood, forming a melt. Beware, violent boiling of reagents can occur in ampoules heated in this way which may lead to rupture. The quartz tube was then put into a furnace and annealed at 250 °C for 3 days. The furnace was

Journal Name ARTICLE

allowed to thermalise to 70  $^{\circ}\text{C}$  before the tube was removed and quenched to room temperature.

#### Characterization

Powder XRD patterns of powders and thin films were acquired on a Bruker D8 Advance Eco Diffractometer using Cu  $K_{\alpha}$  radiation ( $\lambda(K_{\alpha 1})=1.5406$  Å;  $\lambda(K_{\alpha 2})=1.5444$  Å). Pawley refinements were carried out using HighScore Plus Analysis software (Version 5.2). IR measurements were performed with a Shimadzu IR Affinity machine equipped with Shimadzu QATR 10. SEM images were taken using a Zeiss Merlin, equipped with a Zeiss Evo for EDX elemental detection. The samples were noncoated, and micrographs were taken using in-lens mode at an accelerating voltage of 6 kV, a working distance of 10 mm and a vacuum level of 1.5–2.9  $\times$  10<sup>-6</sup> mbar. Elemental compositions were analysed using the Oxford Instruments AZtec analysis software. UV-Vis absorption spectra were measured with a Shimadzu UV-2600 UV-Vis Spectrometer under ambient condition.

#### **Author contributions**

R. L. Z. H. conceived of this work. E. L. Q. and E. T. synthesised the thin films and performed formal analysis under supervision of R. L. Z. H. H. L. undertook theory/computation sections and associated analysis, supervised by A.W. H. L. also performed the solid-state synthesis and characterization. S. D. performed the SEM and EDX measurements. All authors contributed to the preparation of the manuscript.

## **Conflicts of interest**

There are no conflicts to declare.

## Data availability

The raw data (both experimental and computational) generated in this paper and the Supplementary Information can be found from the Oxford University Research Archive (ORA) Data Repository, with the link DOI: XXXXX.

### **Acknowledgements**

The authors are thankful to Prof. Chris Pickard for providing access to updated versions of the EDDP suite, as well as Dr. Peter Cooke for providing useful advice for training EDDPs and general troubleshooting. The authors thank Prof. Simon Clarke for his advice regarding the synthesis of CsBiSCl<sub>2</sub>.The authors thank the UK Research and Innovation for support through a Frontier Grant (no. EP/X029900/1), awarded through the 2021 ERC Starting Grant scheme. E. L. Q. acknowledges funding from the EPSRC Centre for Doctoral Training in Inorganic Chemistry for Future Manufacturing (OxICFM; no. EP/S023828/1). H. L. thanks the Department of Chemistry at the University of Oxford for financial support. S. D. and R. L. Z. H. thank First Solar for financial support. R. L. Z. H. thanks the Royal Academy of

Engineering and Science & Technology Facilities of the RCSRF/23244 18-68).

## References

- J. Y. Kim, J.-W. Lee, H. S. Jung, H. Shin and N.-G. Park, Chem. Rev., 2020, 15, 7867–7918
- 2 C. He. and X. Liu, Light Sci. Appl., 2023, 12, 15.
- 3 T. C. Sum, N. Mathews, G. Xing, S. S. Lim, W. K. Chong, D. Giovanni and H. A. Dewi, Acc. Chem. Res., 2016, 49, 294–302.
- 4 Interactive Best Research-Cell Efficiency Chart | Photovoltaic Research | NREL, https://www.nrel.gov/pv/interactive-cell-efficiency.html, (accessed March 2025).
- 5 A. H. Slavney, T. Hu, A. M. Lindenberg and H. I. Karunadasa, J. Am. Chem. Soc., 2016, 138, 2138–2141.
- D. He, P. Chen, J. A. Steele, Z. Wang, H. Xu, M. Zhang, S. Ding,
  C. Zhang, T. Lin, F. Kremer, H. Xu, M. Hao and L. Wang, *Nat. Nanotechnol.*, 2025, 20, 779–786.
- 7 Y. T. Huang, S. R. Kavanagh, M. Righetto, M. Rusu, I. Levine, T. Unold, S. J. Zelewski, A. J. Sneyd, K. Zhang, L. Dai, A. J. Britton, J. Ye, J. Julin, M. Napari, Z. Zhang, J. Xiao, M. Laitinen, L. Torrente-Murciano, S. D. Stranks, A. Rao, L. M. Herz, D. O. Scanlon, A. Walsh and R. L. Z. Hoye, *Nat. Commun.*, 2022, 13, 4960.
- I. Mosquera-Lois, Y. T. Huang, H. Lohan, J. Ye, A. Walsh and R.
  L. Z. Hoye, *Nat. Rev. Chem.*, 2025, 9, 287–304.
- M. S. Hammer, H. Schlott, L. Lüer, C. J. Brabec, M. Sytnyk, J. Will, B. Meyer and W. Heiss, *Nat. Rev. Mater.*, 2025, **10**, 311–325.
- E. Wlaźlak, A. Blachecki, M. Bisztyga-Szklarz, S. Klejna, T. Mazur, K. Mech, K. Pilarczyk, D. Przyczyna, M. Suchecki, P. Zawal and K. Szaciłowski, Chem. Commun., 2018, 54, 12133–12162.
- 11 U. V. Ghorpade, M. P. Suryawanshi, M. A. Green, T. Wu, X. Hao and K. M. Ryan, *Chem. Rev.*, 2023, **123**, 327–378.
- 12 F. Palazon, Sol. RRL, 2022, 6, 2100829.
- 13 R. E. Brandt, V. Stevanović, D. S. Ginley and T. Buonassisi, MRS Commun., 2015, 5, 265–275.
- 14 F. Giustino and H. J. Snaith, ACS Energy Lett., 2016, 1, 1233– 1240.
- 15 W. Ke and M. G. Kanatzidis, Nat. Commun., 2019, 10, 965.
- I. Ahmed, K. Prakash and S. M. Mobin, Chem. Commun., 2025, 61, 6691–6721.
- 17 J. Huang, H. Wang, C. Jia, H. Yang, Y. Tang, K. Gou, Y. Zhou and D. Zhang, *J. Phys. Chem. Lett.*, 2024, **15**, 3383–3389.
- 18 A. Kojima, K. Teshima, Y. Shirai and T. Miyasaka, J. Am. Chem. Soc., 2009, 131, 6050–6051.
- M. M. Lee, J. Teuscher, T. Miyasaka, T. N. Murakami and H. J. Snaith, *Science*, 2012, 338, 643–647.
- 20 J. P. Correa-Baena, M. Saliba, T. Buonassisi, M. Grätzel, A. Abate, W. Tress and A. Hagfeldt, Science, 2017, 358, 739–744.
- 21 M. A. Green, A. Ho-Baillie and H. J. Snaith, *Nat. Photonics*, 2014, **8**, 506–514.
- 22 H. Dong, C. Ran, W. Gao, M. Li, Y. Xia and W. Huang, *eLight*, 2023. **3**. 3.
- 23 Directive 2011/65/EU of the European Parliament and of the Council, <a href="https://eur-lex.europa.eu/eli/dir/2011/65/oj/eng">https://eur-lex.europa.eu/eli/dir/2011/65/oj/eng</a>, (accessed July 2025).
- 24 V. Pecunia, L. G. Occhipinti and R. L. Z. Hoye, *Adv. Energy Mater.*, 2021, **11**, 2100698.
- 25 G. K. Grandhi, G. Koutsourakis, J. C. Blakesley, F. De Rossi, F. Brunetti, S. Öz, A. Sinicropi, M. L. Parisi, T. M. Brown, M. J. Carnie, R. L. Z. Hoye and P. Vivo, *Nat. Rev. Clean Technol.*, 2025, 1, 132–147.

2025. Downloaded on 04/11/25 22:34:50.

**ARTICLE Journal Name** 

- 26 K. R. Dudipala, T. H. Le, W. Nie and R. L. Z. Hoye, Adv. Mater., 2024. 36. 2304523.
- 27 H. Zhu, I. Turkevych, H. Lohan, P. Liu, R. W. Martin, F. C. P. Massabuau and R. L. Z. Hoye, Int. Mater. Rev., 2024, 69, 19-
- 28 L. Mao, W. Ke, L. Pedesseau, Y. Wu, C. Katan, J. Even, M. R. Wasielewski, C. C. Stoumpos and M. G. Kanatzidis, J. Am. Chem. Soc., 2018, 140, 3775-3783.
- Y. Y. Sun, J. Shi, J. Lian, W. Gao, M. L. Agiorgousis, P. Zhang and S. Zhang, Nanoscale, 2016, 8, 6284–6289.
- 30 R. Nie, A. Mehta, B. W. Park, H. W. Kwon, J. Im and S. Il Seok, J. Am. Chem. Soc., 2018, 140, 872-875.
- 31 C. Zhang, S. Teo, Z. Guo, L. Gao, Y. Kamata, Z. Xu and T. Ma, Chem. Lett., 2019, 48, 249-252.
- 32 F. Hong, B. Saparov, W. Meng, Z. Xiao, D. B. Mitzi and Y. Yan, J. Phys. Chem. C, 2016, 120, 6435-6441.
- 33 D. Quarta, D. M. Tobaldi and C. Giansante, J. Phys. Chem. Lett., 2024, **15**, 7645-7651.
- L. M. Antunes, K. T. Butler and R. Grau-Crespo, Nat. Commun., 2024, **15**, 10570.
- 35 D. Quarta, S. Toso, A. Fieramosca, L. Dominici, R. Caliandro, A. Moliterni, D. M. Tobaldi, G. Saleh, I. Gushchina, R. Brescia, M. Prato, I. Infante, A. Cola, C. Giannini, L. Manna, G. Gigli and C. Giansante, Chem. Mat., 2023, 35, 9900-9906.
- 36 C. Ming, Z. Chen, F. Zhang, S. Gong, X. Wu, J. Jiang, T. Ye, Q. Xu, K. Yang, L. Wang, X. Cao, S. Yang, S. Zhang, Y. Zhang, J. Shi and Y. Y. Sun, Adv. Funct. Mater., 2022, 32, 2112682.
- M. Singh, N. Akash and J. P. Tiwari, ACS Appl. Energy Mater., 2024, **7**, 10212–10229.
- 38 M. Khan, X. Sun, M. Kashif, A. Zada, S. Azizi, A. H. Ragab, M. A. Taher, Q. Abbas and K. Shehzad, Coord. Chem. Rev., 2025, **538**, 216687.
- 39 D.-A. Park and N.-G. Park, SusMat, 2025, 5, e70018.
- 40 M. H. Miah, M. U. Khandaker, M. J. Hossen, N. Noor-E-Ashrafi, I. Jahan, M. Shahinuzzaman, M. Nur-E-Alam, M. Y. Hanfi, M. H. Ullah and M. A. Islam, *Mater. Adv.*, 2025, **6**, 2718–2752.
- 41 A. Jain, S. P. Ong, G. Hautier, W. Chen, W. D. Richards, S. Dacek, S. Cholia, D. Gunter, D. Skinner, G. Ceder and K. A. Persson, APL Mater., 2013, 1, 11002.
- 42 M. K. Horton, P. Huck, R. X. Yang, J. M. Munro, S. Dwaraknath, A. M. Ganose, R. S. Kingsbury, M. Wen, J. X. Shen, T. S. Mathis, A. D. Kaplan, K. Berket, J. Riebesell, J. George, A. S. Rosen, E. W. C. Spotte-Smith, M. J. McDermott, O. A. Cohen, A. Dunn, M. C. Kuner, G. M. Rignanese, G. Petretto, D. Waroquiers, S. M. Griffin, J. B. Neaton, D. C. Chrzan, M. Asta, G. Hautier, S. Cholia, G. Ceder, S. P. Ong, A. Jain and K. A. Persson, Nat. Mater., 2025, 24, 1522-1532.
- 43 B. Deng, P. Zhong, K. J. Jun, J. Riebesell, K. Han, C. J. Bartel and G. Ceder, Nat. Mach. Intell., 2023, 5, 1031–1041.
- 44 H. Yang, C. Hu, Y. Zhou, X. Liu, Y. Shi, J. Li, G. Li, Z. Chen, S. Chen, C. Zeni, M. Horton, R. Pinsler, A. Fowler, D. Zügner, T. Xie, J. Smith, L. Sun, Q. Wang, L. Kong, C. Liu, H. Hao and Z. Lu, Preprint arXiv arXiv:2405.04967, 2024.
- 45 C. J. Pickard, *Phys. Rev. B*, 2022, **106**, 014102.
- 46 C. J. Pickard, Faraday Discuss., 2025, 256, 61-84.
- W. Ke, I. Spanopoulos, C. C. Stoumpos and M. G. Kanatzidis, Nat. Commun., 2018, 9, 4785.
- 48 W. M. Linhart, S. J. Zelewski, P. Scharoch, F. Dybała and R. Kudrawiec, J. Mater. Chem. C, 2021, **9**, 13733–13738.
- 49 H. Zhang, J. Diao, M. Ouyang, H. Yadegari, M. Mao, J. Wang, G. Henkelman, F. Xie, D. J. Riley, H. Zhang, H. Yadegari, F. Xie, D. J. Riley, J. Diao, J. Wang, G. Henkelman, M. Ouyang and M. Mao, Adv. Funct. Mater., 2022, 32, 2205974.
- 50 N. Huang, C. Yao, J. Cheng, F. Yu, Y. Zhao, F. Li, Y. Ou and L. Liu, Next Materials, 2024, 4, 100222.
- 51 Y. Xiao, H. Jiang, K. Zhang, Y. Kong, S. Zhang, H. Wang, G. Yuan, D. Su, J. Zhou, X. Wang, L. Xin, A. Wang and S. Fang, Chem. Eng. J., 2024, 492, 152274.

- 52 P. Liu, DPhil Thesis, University of Oxford, 2024. View Article Online 53 S. Rieger, B. J. Bohn, M. Döblinger, A. Fo Richters / Stephenson Wang, P. Müller-Buschbaum, L. Polavarapu, L. Leppert, J. K. Stolarczyk and J. Feldmann, *Phys. Rev. B*, 2014, **100**, 201404.
- 54 D. Prochowicz, P. Yadav, M. Saliba, D. J. Kubicki, M. M. Tavakoli, S. M. Zakeeruddin, J. Lewiński, L. Emsley and M. Grätzel, Nano Energy, 2018, 49, 523-528.
- 55 Y. Jia, R. Li, Y. Zhou, S. Zhao, H. Yu, J. Wang, Z. Lin, H. Su and N. Zhao, Small Struct., 2023, 4, 2200393.
- 56 A. Kirakosyan, Y. Kim, M. R. Sihn, M. G. Jeon, J. R. Jeong and J. Choi, ChemNanoMat, 2020, 6, 1863-1869.
- 57 A. J. Cohen and R. G. Gordon, Phys. Rev. B, 1975, 12, 3228.
- 58 H. Zhang, S. H. Sun, J. C. Liu, F. Hong, Y. Zhu, B. Zhou and Y. M. Hu, Nano, 2020, 15, 2050116.
- 59 C. J. Pickard, Phys. Rev. B, 2022, 106, 014102.
- 60 P. T. Salzbrenner, S. H. Joo, L. J. Conway, P. I. C. Cooke, B. Zhu, M. P. Matraszek, W. C. Witt and C. J. Pickard, J. Chem. Phys., 2023, **159**, 144801.
- 61 C. J. Pickard and R. J. Needs, J. Phys.: Condens. Matter, 2011, **23**. 053201.
- 62 S. P. Ong, L. Wang, B. Kang and G. Ceder, Chem. Mat., 2008, **20**. 1798–1807.
- 63 A. Jain, G. Hautier, S. P. Ong, C. J. Moore, C. C. Fischer, K. A. Persson and G. Ceder, Phys. Rev. B, 2011, 84, 045115.
- 64 S. J. Clark, M. D. Segall, C. J. Pickard, P. J. Hasnip, M. I. J. Probert, K. Refson and M. C. Payne, Zeitschrift fur Kristallographie, 2005, **220**, 567–570.
- 65 J. P. Perdew, A. Ruzsinszky, G. I. Csonka, O. A. Vydrov, G. E. Scuseria, L. A. Constantin, X. Zhou and K. Burke, Phys. Rev. Lett., 2008, 100, 136406.
- 66 E. Caldeweyher, S. Ehlert, A. Hansen, H. Neugebauer, S. Spicher, C. Bannwarth and S. Grimme, J. Chem. Phys., 2019, 150, 154122.
- 67 S-H. Joo dpp-batch, https://github.com/SehunJoo/ddp-batch, (accessed September 2025).
- 68 J. W. Furness, A. D. Kaplan, J. Ning, J. P. Perdew and J. Sun, J. Phys. Chem. Lett., 2020, 11, 8208-8215.
- 69 S. Grimme, S. Ehrlich and L. Goerigk, J. Comput. Chem., 2011, 32, 1456-1465.
- 70 G. Kresse and J. Hafner, Phys. Rev. B, 1993, 47, 558.
- 71 G. Kresse and J. Furthmüller, Phys Rev B, 1996, 54, 11169.
- 72 G. Kresse and D. Joubert, *Phys Rev B*, 1999, **59**, 1758.
- 73 A. J. Jackson, kgrid, https://github.com/WMD-group/kgrid, (accessed September 2025).
- 74 A. Togo, J. Phys. Soc. Jpn., 2023, 92, 012001.
- 75 A. Togo, L. Chaput, T. Tadano and I. Tanaka, J. Phys.: Condens. Matter, 2023, **35**, 353001.

**EES Solar Accepted Manuscript** 

# **Data Availability Statement**

View Article Online DOI: 10.1039/D5EL00157A

The raw data (both experimental and computational) generated in this paper and the Supplementary Information can be found from the Oxford University Research Archive (ORA) Data Repository, with the link DOI: XXXXX.